JTTEE5 5:335-342

Comparison between Ni-Cr-40vol%TiC Wear-Resistant Plasma Sprayed Coatings Produced from Self-Propagating High-Temperature Synthesis and Plasma Densified Powders

C. Bartuli and R.W. Smith

Plasma sprayed Ni-Cr-40vol% TiC coatings produced from powders obtained by self-propagating high-temperature synthesis (SHS) and plasma densification (PD) processes are characterized. Chemical composition, microstructure, and mechanical properties, such as microhardness and wear resistance, are evaluated and compared. SHS coatings exhibit good sliding wear performance.

The exact stoichiometry of titanium carbide inclusions in the metallic matrix affects the dimension of the crystal lattice parameter and was investigated by examining the shift of x-ray diffraction (XRD) peaks of the TiC. A value of the combined carbon/titanium ratio of about 0.6 was calculated for both powders, thus excluding the influence of the stoichiometry of the carbide inclusions on the wear properties of the coatings.

Keywords Ni-Cr coatings, self-propagating high-temperature synthesis (SHS), sliding wear, substoichiometry, titanium carbide

1. Introduction

PLASMA SPRAYED dispersion hardened metallic coatings are widely used for improving wear resistance of surfaces. Carbides are very effective as reinforcement materials. They are able to toughen more ductile matrices and, therefore, reduce the wear caused by sliding erosion.

In particular, titanium carbide shows very good performance, especially in severe temperature operating conditions where chromium or tungsten carbides, successfully employed elsewhere, can decompose and become ineffective (Ref 1).

In the present paper, oxidation and corrosion-resistant plasma sprayed Ni-Cr coatings, alloyed with small quantities of secondary constituents (such as Fe and Ti), and reinforced by TiC dispersions, are characterized. In particular, features and performances of coatings produced from conventional PD powders are compared with those of coatings deposited from SHS powders (Ref 2).

Self-propagating high-temperature synthesis (SHS) (Ref 3, 4) is a combustion process in which an exothermic, self-sustaining chemical reaction proceeds layer by layer into the reaction volume, gradually transforming the reactant powder mixture into the desired products. The energy necessary for the synthesis of refractory compounds is self-generated by the heat of reaction, thus avoiding the need to maintain high temperatures for long times in furnaces. Also, the equipment used for the SHS process is usually very simple, thus dramatically reducing the initial costs with respect to conventional methods.

The kinetics of the combustion reaction, the structure and the velocity of the combustion wave, and the mechanism of the reactions taking place during an SHS process are related to the adiabatic temperature (T_{ad}), which is defined as "the maximum temperature to which the products are raised under adiabatic conditions as a consequence of the evolution of heat during the chemical reaction" (Ref 5).

Figure 1 is a schematic representation of a SHS reaction. After ignition with an external source (for example electric arc, laser, tungsten heating coil, oxyacetylene torch), reactants and

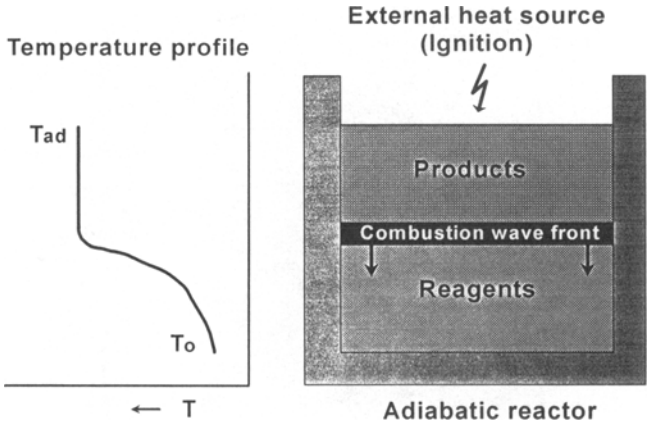

Fig. 1 Schematic representation of a SHS process. The temperature profile, which originates in the reaction volume (from ambient temperature, T_0, to the adiabatic temperature, T_{ad}), is indicated on the left side, where the vertical axis refers to the location along the center line of the adiabatic reactor.

C. Bartuli, Department of ICMMPM, University "La Sapienza," Rome, Italy; and **R.W. Smith,** Center for Plasma Processing of Materials, Department of Materials Engineering, Drexel University, Philadelphia PA, USA.

products are separated by a combustion wave front moving through the reaction volume with a constant velocity.

2. Experimental

2.1 *Powder Production Techniques*

SHS powders of the nominal composition 31Ni-17Cr-6.8Fe-2.9Ti-2.5Al-39TiC (vol%) supplied by Exotherm Corporation, Camden, NJ, were produced by reacting compacted elemental blends of reactants (Ni, Cr, Fe, Al, Ti, C) of different initial size (<325 mesh for the metals, <1 μm for the carbon black) prepressed into 8 cm diameter cylindrical pellets in a reactor with thermally insulated walls under an argon atmosphere.

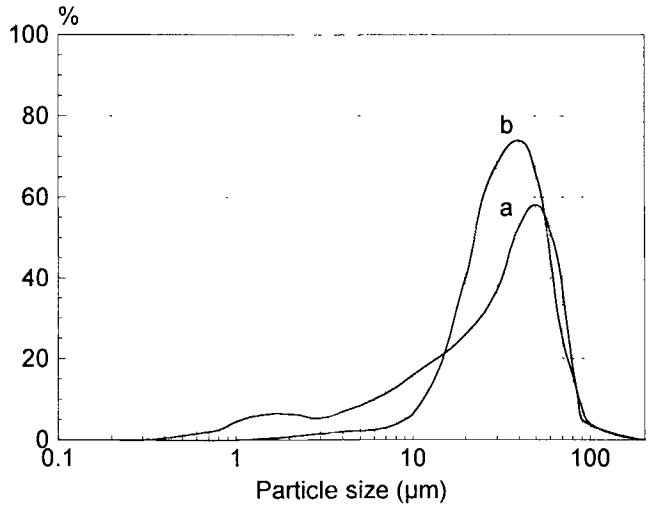

Fig. 2 Particle size distributions for (curve a) SHS and (curve b) PD powders

Initial density of the pellets was 50% of the theoretical density. Ignition was carried out with a tungsten filament. A small quantity (less than 0.3 wt%) of a proprietary additive was added to the initial mixture to modify the wetting characteristics of the SHS process and control the velocity of propagation of the reaction front.

A combustion temperature of 1450 °C was attained during the reaction, proceeding with a combustion rate of 0.18 cm/s. Products of the synthesis (about 60% dense) were milled and screened to the final nominal size (<270 mesh).

Commercially available powders (Ferro-TiC Resistic Grade HT6A, supplied by Alloy Technology International, Inc., Nyack, NY) of similar composition, 39Ni-12.5Cr-5.3Fe-1.5Ti-40TiC (vol%), <325 mesh and >15 μm, produced by conventional plasma densification (PD) were characterized and compared to the SHS product.

2.2 *Powder Characterization*

Size distribution of the particles was investigated by laser light scattering Malvern Mastersizer (Malvern Instruments, Southborough, MA) in a liquid dispersant (distilled water). The water containing the powder sample was stirred during measurement, and ultrasonic agitation was applied for ~1 min in the case of SHS powders to dissolve clusters or physical aggregates of particles. The instrument assumes a round shape of all particles.

The general morphology of the powders was characterized by scanning electron microscopy (SEM) (Philips SEM 505, Philips Electronics North America, New York; 20 to 25 kV accelerating tension).

X-ray diffraction (XRD) analyses were performed on samples from the as-supplied powders to investigate the presence of undesired compounds or phases possibly formed during the synthesis reaction and to evaluate and compare the actual carbon content in the TiC_{1-x} present in the SHS and PD powders (Ref 6, 7). A Siemens D500 diffractometer (Siemens Analytical X-Ray

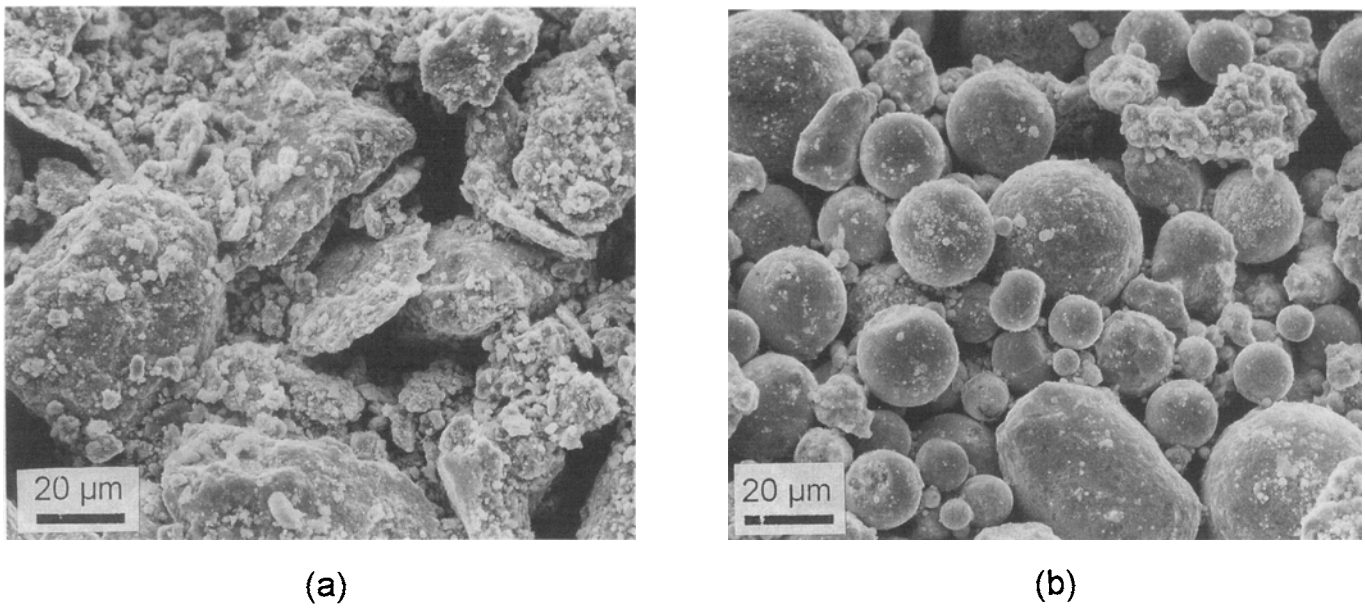

Fig. 3 SEM micrographs of (a) SHS and (b) PD powders

Instruments Inc., Madison, WI) was used for all measurements, selecting the copper Kα radiation filtered with nickel. The interval of 2θ diffraction angle ranging from 20° to 120° was investigated with a scanning step of 0.05° and a scanning time of 1 s. An internal standard of pure silicon was used.

2.3 *Deposition Parameters*

Air (APS) and vacuum (VPS) plasma spray coatings were deposited onto grit-blasted 4140 stainless steel coupons (25 by 75 by1.5 mm). 4140 steel discs (70 mm diameter by 2 mm) were also coated for sliding wear resistance evaluation. Spray parameters are summarized in Table 1.

2.4 *Coating Characterization*

Metallographic samples from the as-sprayed coatings were obtained by the following polishing procedure: 300 mesh silicon carbide grinding paper and 3 μm diamond impregnated discs. The use of finer SiC abrasive paper was avoided to limit the pullout of titanium carbide inclusions from the metallic matrix.

SEM analyses were performed under the same operating conditions described above to characterize the substrate-coating and matrix-inclusion interfaces. Energy dispersive spectroscopy (EDS) was used for chemical elemental analysis.

X-ray diffraction analyses of whole samples of the coatings were also carried out to identify changes of either the chemical or phase composition during plasma spraying and to investigate the presence of residual stresses in the coatings.

Coatings were finally characterized on the basis of their microhardness and wear resistance. For microhardness measurements on polished sections of the coatings, a LECO M400 Vickers microindentator (LECO Corporation, St. Joseph, MD) was used with a load of 300 g applied for 10 s.

Unlubricated pin-on-disc sliding wear testing was performed in dry air on ground and polished plasma sprayed coatings on

Table 1 Air plasma spray (APS) and vacuum plasma spray (VPS) parameters for self-propagating high-temperature synthesis (SHS) and plasma densified (PD) coatings

Powder	Atmosphere		Plasma gas 1 (argon), scfh	Plasma gas 2 (helium), scfh	Carrier gas (argon), scfh	Spray distance, cm	Arc current, A	Arc voltage, V	Coating thickness, mm
	Type	Torr							
SHS	APS	760	125	60	27	9	1000	38	0.35
	VPS	200	140	70	18	17.5	1100	47	0.35
PD	APS	760	140	70	18	9	1100	38	0.47
	VPS	200	140	60	18	17.5	1100	50	0.27

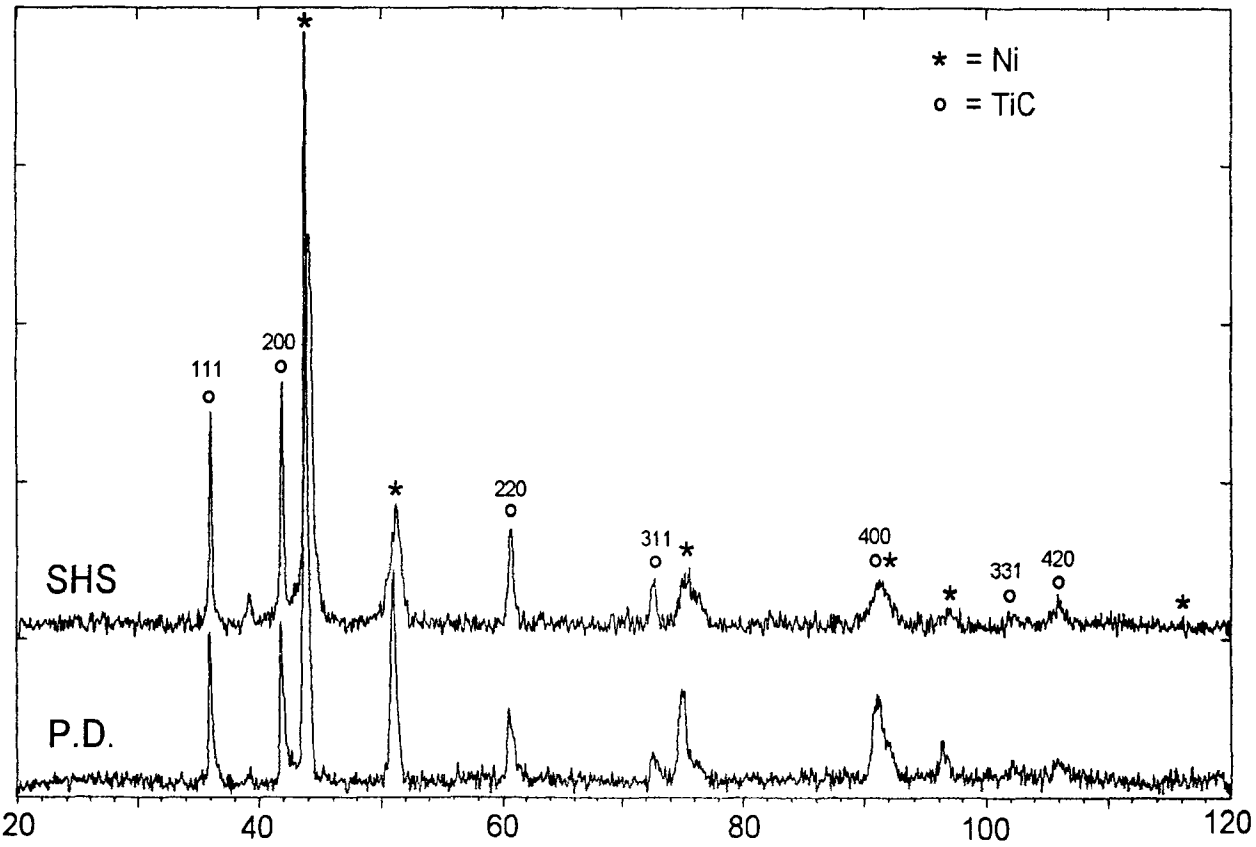

Fig. 4 XRD patterns of as-supplied SHS and PD powders

discs (ASTM G99-90 testing procedure). The sliding counterbody was an Al_2O_3 (sapphire) ball of 10 mm diameter. A normal load of 20 to 30 N was applied, and a coating/counterbody relative velocity of 0.44 m/s was set. Wear tracks after 10,000 cycles were observed, and areas were measured by a steel stylus profilometer.

3. Results and Discussion

3.1 *Powders*

Size distributions of the SHS and PD powders, as obtained by laser light scattering, are illustrated in Fig. 2. The SHS powder distribution is wide and almost bimodal. In particular, 55% of the particles fall in the 20 to 80 μm range, distributed around the highest peak, at about 50 μm. A further 20% of the particles fall in the 0.5 to 10 μm range, more or less distributed around the second peak, at about 2 μm. Ultrasonic agitation was applied for 1 min for better dispersion. Note that the "tail" of the Gaussian distribution of these powders toward the low sizes cannot be eliminated by mechanical sieving, and air classification is recommended.

The narrower and more regular size distribution of the PD powders is exhibited for comparison; about 80% of the particles are in the 20 the 80 μm range. SEM micrographs of the powders in Fig. 3 show that SHS powders are fragmented and angular shaped (Fig. 3a). Fine particles (about 1-2 μm) are distributed on the surface and among larger grains (20-30 μm). The more spherical morphology of the PD powder is shown in Fig. 3(b).

As expected on the basis of the results illustrated, the flowability of the SHS powder—in particular its ability to flow through a given nozzle at given pressure (80 psi) and feeder rotation (3 rpm)—as compared to the PD, is low. Experiments indicate a flowability of 23 g/min for the SHS powder compared to 38 g/min for the PD material.

X-ray diffraction patterns of typical SHS and PD powders are shown in Fig. 4. Peaks corresponding to the characteristic lines

Table 2 Diffraction pattern of stoichiometric $TiC_{1.0}$

Interplanar spacing (d), nm	Plane h	k	l
0.24990	1	1	1
0.21637	2	0	0
0.15302	2	2	0
0.13047	3	1	1
0.12492	2	2	2
0.10818	4	0	0
0.09927	3	3	1
0.09677	4	2	0
0.08834	4	2	2
0.08327	5	1	1

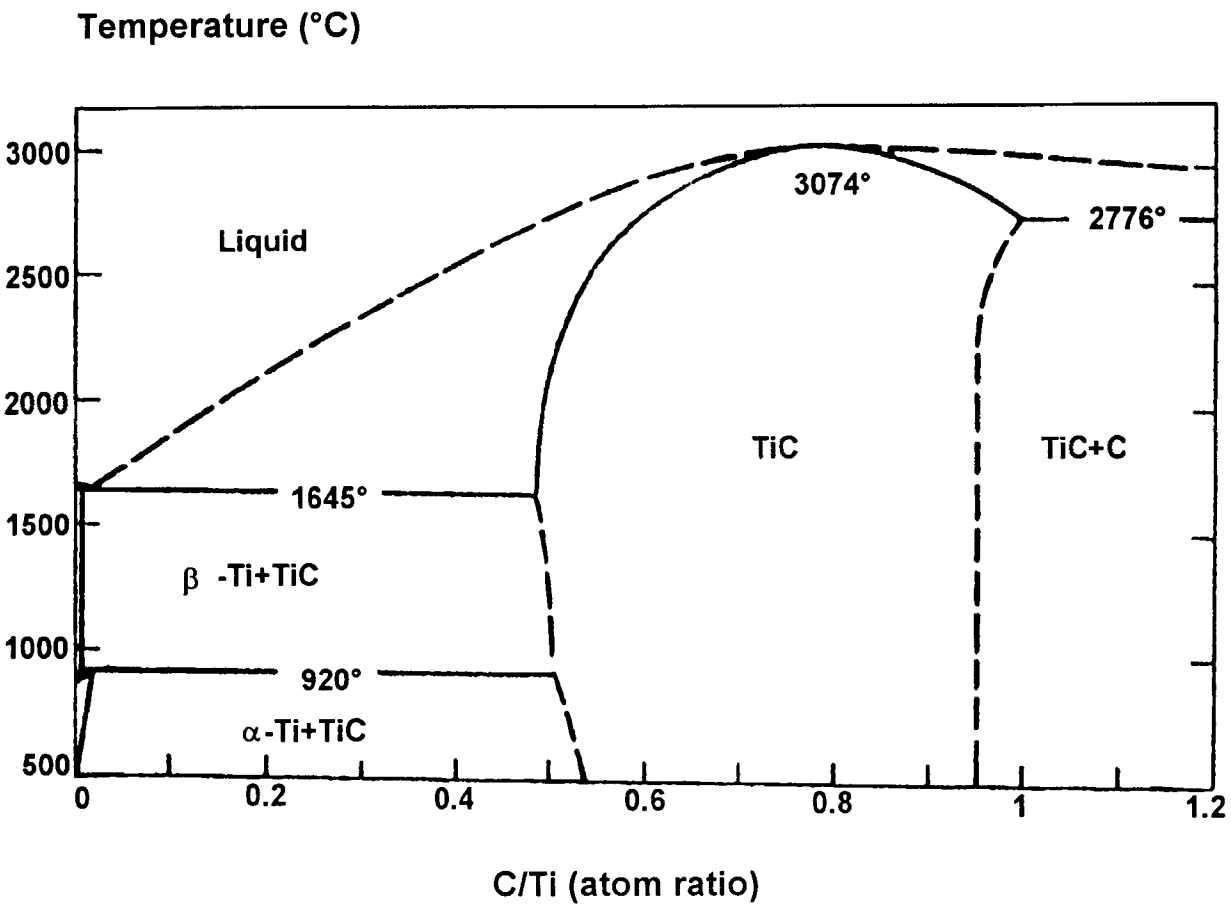

Fig. 5 Carbon/titanium phase diagram (Ref 8)

of nickel and titanium carbide are clearly identified in both cases. Most of the chromium characteristic lines are covered by the nickel pattern.

Using the same analytical technique, a detailed investigation was also carried out on the crystalline structure of the titanium carbide present in the powders to identify its exact stoichiometry. Titanium carbide (Ref 8), TiC, is usually a stoichiometric compound characterized by a face-centered cubic lattice (Ref 9) identified by a single lattice parameter, a. However, this carbide can also exist over a wide range of substoichiometries. The phase diagram of the C/Ti system is shown in Fig. 5 (Ref 8).

A correlation can be established (Ref 9-11) between the value of the lattice parameter of TiC_{1-x} and the atomic ratio of the combined carbon over titanium (that is, the value of $1 - x$); see Fig. 6 (Ref 9). The lattice parameter of a crystalline compound can be

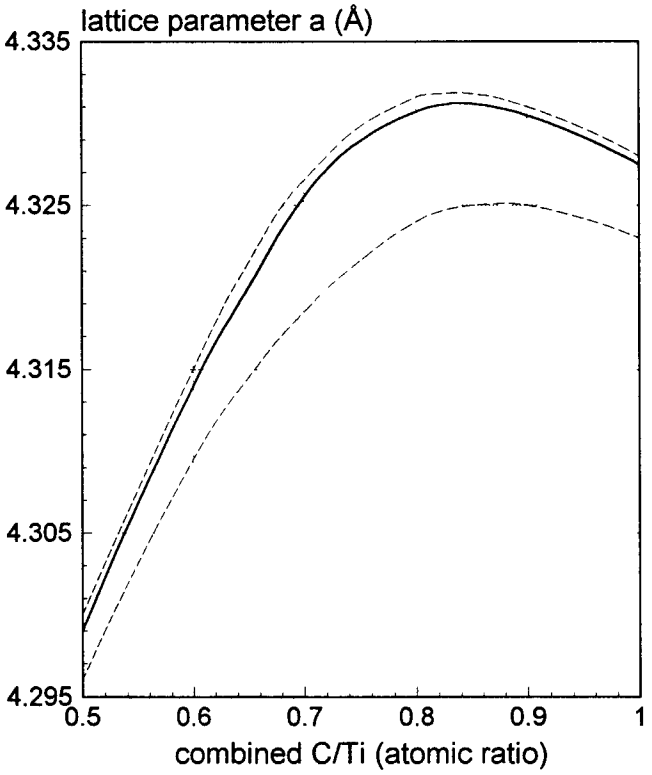

Fig. 6 Lattice parameter a of TiC_{1-x} as a function of the C/Ti ratio (adapted from Ref 9)

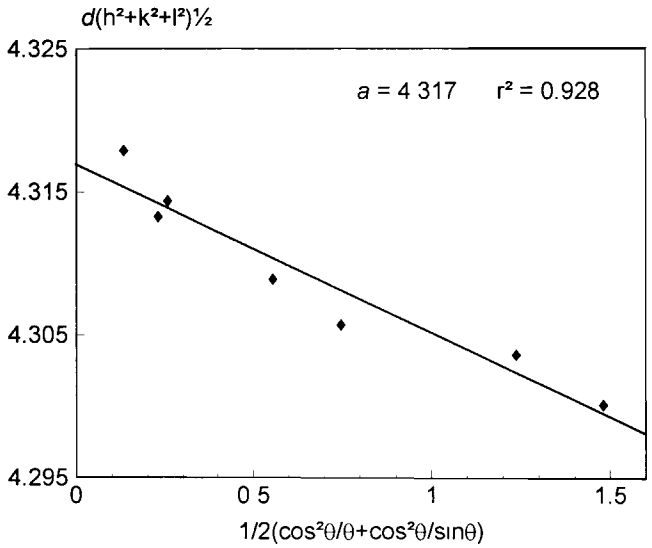

Fig. 7 Example of construction of the $[d(h^2 + k^2 + l^2)^{1/2}]$ versus $[\frac{1}{2}(\cos^2\theta/\theta + \cos^2\theta/\sin\theta)]$ plot for the determination of the lattice parameter of the SHS powder for one particular XRD run. The values of the intercept with the ordinates axis, a, and of the correlation coefficient, r^2, are indicated.

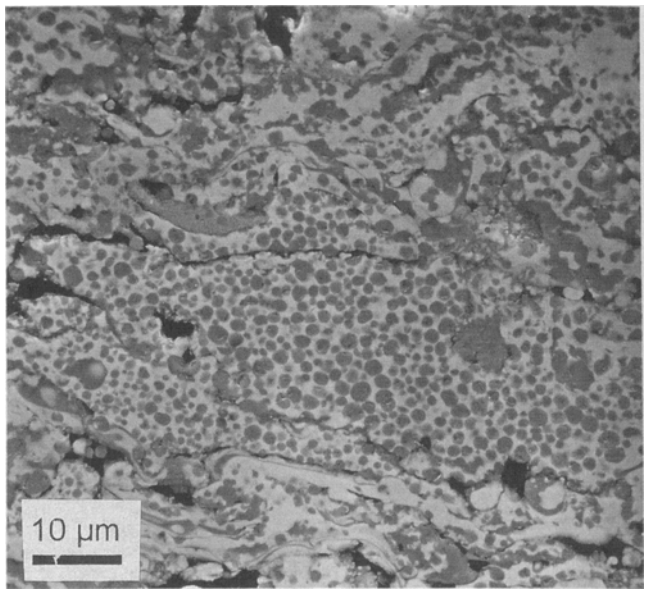

(a)

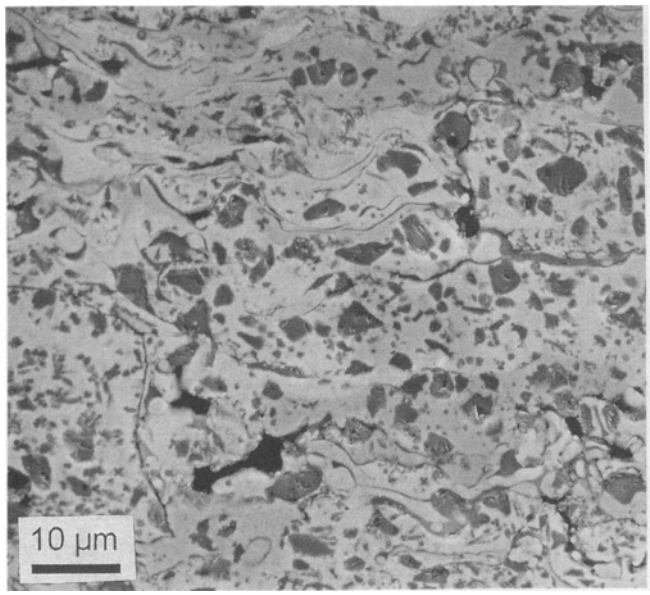

(b)

Fig. 8 SEM micrographs of APS coatings produced from (a) SHS and (b) PD powders

directly correlated to the value of the interplanar spacings, d, and the corresponding 2θ angles of the peaks identifying its characteristic XRD pattern.

The calculated positions of the diffraction lines for stoichiometric $TiC_{1.0}$ are listed in Table 2 (Ref 12). The corresponding value of lattice parameter, a, is 0.43270 nm.

The values of parameter a calculated from the measured diffraction patterns of six samples from the SHS powder and six samples from the PD powder were compared. The final value of a for each diffraction run was extrapolated for 2θ angles approaching 180° since large Bragg angles are much more sensitive to small changes in cell dimension (Ref 13). To this aim, for each value of the measured d spacing, the value of $[d\,(h^2 + k^2 + l^2)^{1/2}]$ was plotted against the corresponding value of $[\frac{1}{2}(\cos^2\theta/\theta + \cos^2\theta/\sin\theta)]$. The resulting points are distributed around a straight line, whose parameters can be calculated by the least squares method. The intercept with the ordinate axis is the final value of a for that diffraction run (Ref 13).

For the present case, d values were measured for only 7 of the 10 lines characteristic of the TiC pattern. In fact, two of the remaining peaks (corresponding to the [2 2 2] and [4 0 0] planar directions) fall very close to some of the peaks generated by Ni, making their attribution unreliable; the last peak (plane [5 1 1]) was not clearly detected by the instrument. In Fig. 7, the construction of the $[d\,(h^2 + k^2 + l^2)^{1/2}]$ versus $[\frac{1}{2}(\cos^2\theta/\theta + \cos^2\theta/\sin\theta)]$ plot used to calculate the lattice parameter of the SHS powder for a single diffraction run is illustrated.

Average values of a were calculated from the six SHS samples and the six PD samples (Table 3) together with their stan-

Table 3 Lattice parameter and C/Ti ratio for SHS and PD powders

Powder	Lattice parameter (a), nm	Standard deviation (σ_a), nm	C/Ti ratio, $1 - x$
SHS	0.43168	0.00012	0.627
PD	0.43165	0.00011	0.623

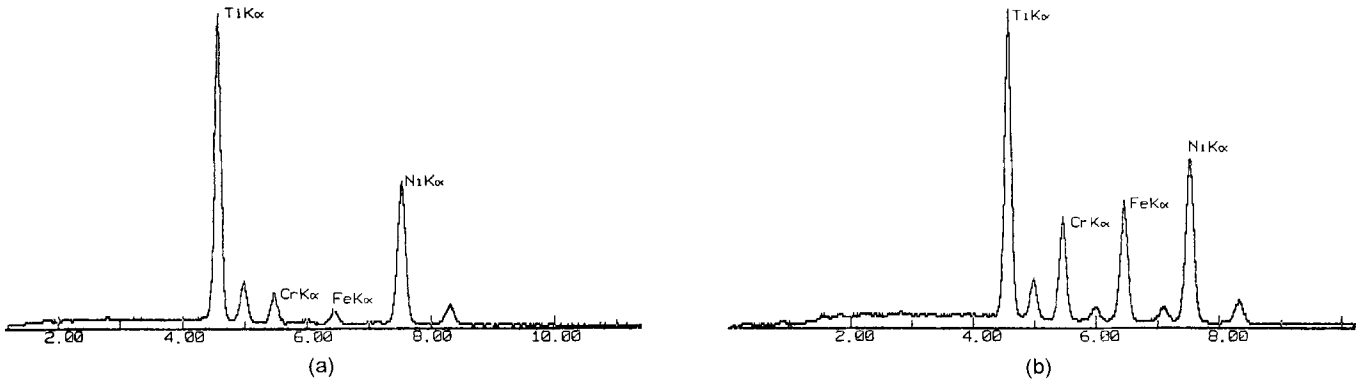

Fig. 9 EDS patterns of APS coatings produced from (a) SHS and (b) PD powders

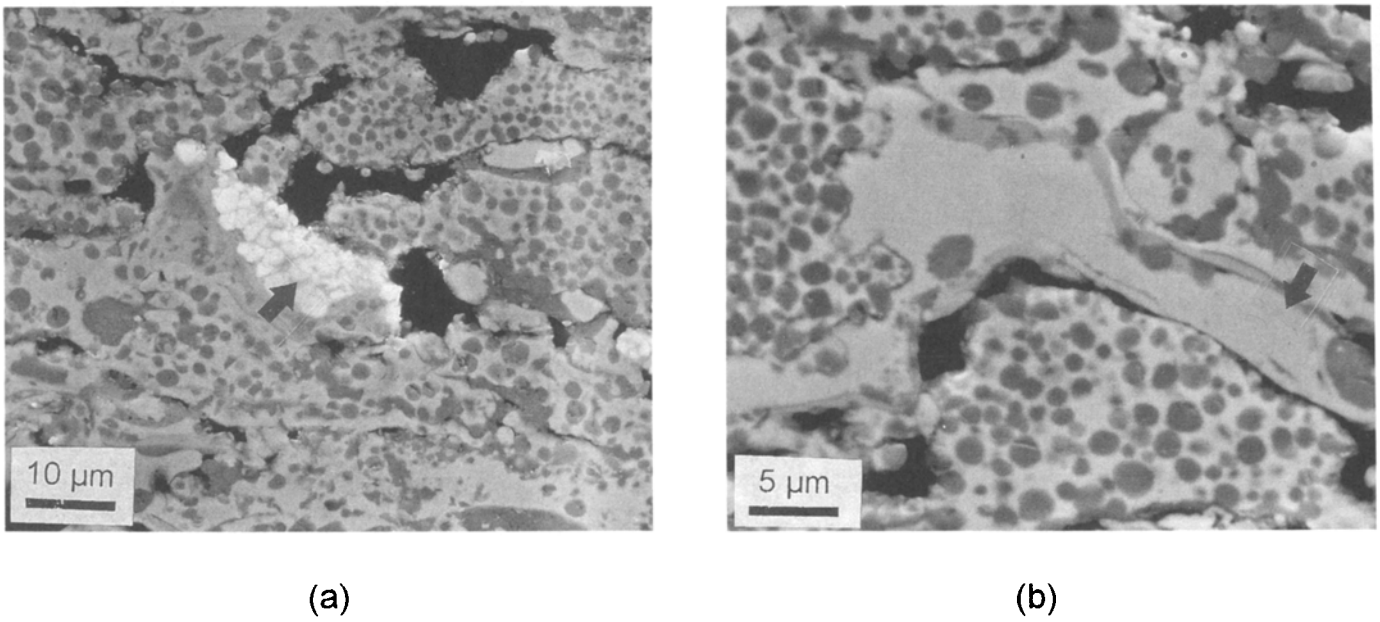

Fig. 10 SEM micrographs of two inclusions (indicated by arrows) in the APS coating produced from SHS powders

dard deviations. The corresponding values of $1-x$ (carbon/titanium atom ratio) calculated from the curve in Fig. 6 are also listed.

The above results show that the stoichiometry of the titanium carbide present in the SHS and PD powders does not differ significantly. Therefore, any possible difference in the microhardness (Ref 14) or other mechanical and wear properties (Ref 15-17) of the coatings produced by the two techniques cannot be attributed in this case to the carbon content of the carbide reinforcement.

3.2 *Coatings*

Figure 8 shows the microstructure of polished cross sections of APS coatings obtained by air plasma spray of SHS (Fig. 8a) and PD (Fig. 8b) powders. Dark areas represent TiC particles (as confirmed by EDS analyses) embedded in the metallic Ni-Cr matrix. The size, shape, and distribution of the carbides are different in each case.

SHS carbides are rounded and generally smaller, ranging from fractions of a micron to 2-3 μm. The nonhomogeneous size and distribution of the carbides in the Ni-Cr matrix depend on the original distribution in the single drops impinging on the substrate. The angular-shaped, more uniformly sized carbides in the PD coating are shown in Fig. 8(b).

Chemical analyses of the APS coatings confirmed the presence of the expected elements, with the prevalence of chromium and iron in the coating produced from PD powders with respect to the SHS (see Fig. 9).

Inclusions of different size and morphology were observed in the SHS coating; see Fig. 10. Elemental analyses indicated the presence of nickel and aluminum rich areas, possibly suggesting the formation and segregation of small quantities of nickel aluminides of different stoichiometries, on the basis of theoretical calculations, as well as areas characterized by a high percentage of iron.

Figure 11 compares XRD patterns of SHS powders (pattern a) and of an SHS coating in the as-sprayed condition (pattern b). The positions of TiC peaks remain unchanged in the two cases confirming that the stoichiometry of titanium carbide is not affected by the spraying process. However, a distinct shift of nickel characteristic peaks in the coating diffraction pattern suggests the presence of a residual stress field within the coating caused by the rapid cooling of the coating constrained on a steel substrate with a different thermal expansion coefficient. The same behavior was observed in the case of PD coatings.

Table 4 summarizes the results of Vickers microindentation measurements for both APS and VPS coatings prepared from SHS and PD powders. No significant differences in the coatings produced under the different conditions from the two types of feedstock are distinguished. On the other hand, as indicated by wear test results for VPS coatings summarized in Table 5, SHS coatings exhibited a much better resistance to sliding abrasion. No significant wear track was observed on the surface of SHS

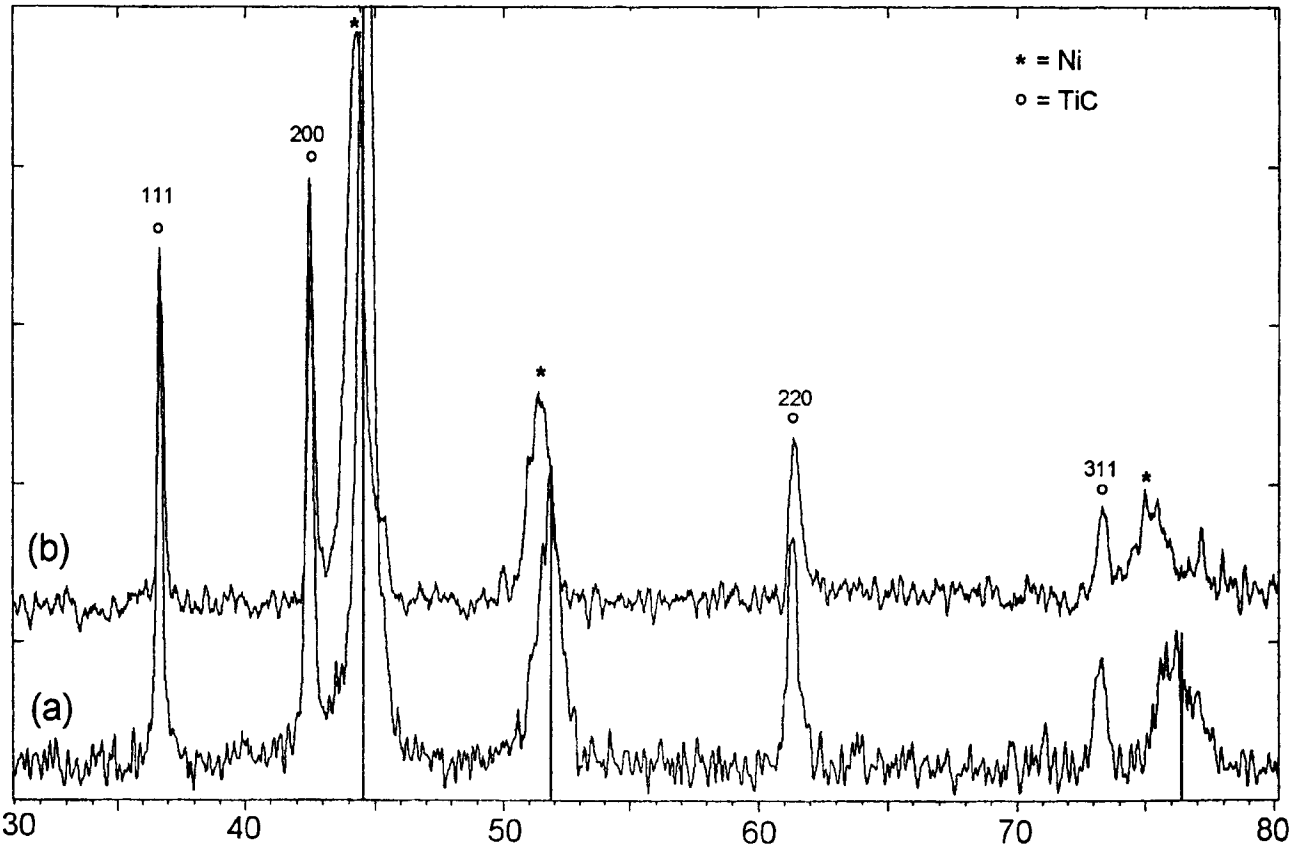

Fig. 11 Comparison between XRD patterns of (a) SHS powders and (b) as-sprayed SHS coating. The position of Ni characteristic lines in a standard pattern is indicated by an asterisk (*).

Table 4 Vickers microhardness test results

Powder	Spray process	HV, kg/mm^2	σ, kg/mm^2
SHS	APS	756	100
	VPS	658	124
PD	APS	727	76
	VPS	717	100

Average of 10 measurements

Table 5 Sliding wear test results for VPS coatings

Powder	Coefficient of friction		Normal load, N	Wear track area, μm^2
	Initial	Final		
SHS	0.45	0.55	30	2764
PD	0.50	0.60	20	1330

discs tested under conditions (normal load of 20 N) sufficient to cause a wear track area of 1330 μm^2 in the PD coating. The normal load had to be increased to 30 N to measure a track area of 2764 μm^2 in the SHS coating.

An explanation of the improved wear behavior of the SHS coatings might be the high quality of the carbide-matrix interface formed during the synthesis process. Furthermore, the morphology of the TiC inclusions can play an important role in the wear mechanism. Round-shaped carbides, such as those observed in the SHS coatings, can reduce—as compared to cutting, angular shaped particles—the damage of the surface caused by the presence of a hard third body (the carbide itself) between the coating and the counterbody.

4. Conclusions

Powders of Ni-Cr-TiC produced by self-propagating high-temperature synthesis can be employed for the deposition of wear-resistant coatings as demonstrated by the comparison of important properties, such as microhardness and resistance to abrasive action under sliding conditions, with those of currently employed plasma densified powders.

The chemical composition of the powder can be controlled satisfactorily. The titanium/carbon ratio in the carbide synthesized by SHS corresponds with that of the products of other synthesis procedures.

The homogeneous distribution of the round-shaped reinforcement particles inside the matrix occurs by the in situ reaction from elements that were originally dispersed in the metal.

Acknowledgments

Mr. Emil Shtessel, Exotherm Corporation, Camden, NJ, USA, is kindly acknowledged for supplying SHS powders and useful detailed information regarding the SHS production process.

References

1. R.W. Smith, D. Gentner, E. Harzenski, and T. Robisch, The Structure and Properties of Plasma Sprayed TiC Dispersion Hardened Coatings, *Thermal Spray Technology: New Ideas & Processes,* D.L. Houck, Ed., ASM International, 1989, p 299-306
2. C. Bartuli, R.W. Smith, and E. Shtessel, Self-Propagating High Temperature Synthesis (SHS) of Ceramic and Composite Powders for Thermal Spray Applications, *Advances in Science and Technology: Advances in Inorganic Films and Coatings,* Vol 5, P. Vincenzini, Ed., Techna, 1995, p 131-140
3. J.W. McCauley, An Historical and Technical Perspective on SHS, *Ceram. Eng. Proc.*, Vol 11, 1990, p 1137-1181
4. A.G. Merzhanov, Self-Propagating High-Temperature Synthesis: Twenty Years of Search and Findings, *Combustion and Plasma Synthesis of High Temperature Materials,* Z.A. Munir and J.B. Holts, Ed., VCH Publishers, 1990, p 1-53
5. J. Subrahmanyam and M. Vijayakumar, Review: Self-Propagating High-Temperature , *J. Mater. Sci.*, Vol 27, 1992, p 6249-6273
6. K.S. Vecchio, J.C. La Salvia, M.A. Meyers, and G.T. Gray III, Microstructural Characterization of Self-Propagating High-Temperature Synthesis/Dynamically Compacted and Hot-Pressed Titanium Carbides, *Metall. Trans. A,* Vol 23, 1992, p 87-97
7. M. Oyanagi, M. Kanno, and M. Koizumi, Characterization of Titanium Carbide (TiC) Formed by SHS, *Int. J. Self. Prop. High Temp. Synth.*, Vol 1 (No. 1), 1992, p 125-130
8. T.Y. Kosolapova, *Carbides: Properties, Production and Applications,* Plenum Press, 1971, p 97-111
9. E.K. Storms, *The Refractory Carbides,* Academic Press, 1967, p 1-17
10. P. Capkova, P. Karen, and L. Dobiasova, Determination of Molar Ratio in AB_{1-x} Rock Salt-Type Compounds by X-Ray Powder Diffraction Method. Application to TiC_{1-x}, *Cryst. Res. Technol.*, Vol 21 (No. 6), 1986, p 735-740
11. L. Reimer, *Transmission Electron Microscopy,* Springer-Verlag, 1984
12. Powder Diffraction File-2 Database, ICDD, 1991, for CD-ROM
13. H. Lipson and H. Steeple, *Interpretation of X-Ray Powder Diffraction Patterns,* St. Martin's, 1970
14. C. Vincent, J. Dazord, H. Vincent, and J. Bouix, Thermodynamic and Experimental Investigation of the Stoichiometry of Titanium Carbide Obtained from the Reaction between a Graphite Substrate and a Gaseous Mixture of Titanium Tetrachloride and Hydrogen, *Thermochim. Acta,* Vol 138, 1989, p 81-96
15. S. Ramalingam, Stoichiometry of Titanium Carbide and Its Significance to the Performance of Hard Metal Compacts, *Mater. Sci. Eng.*, Vol 29, 1977, p 123-130
16. S. Tsurekawa, H. Kurishita, and H. Yoshinaga, High Temperature Deformation Mechanism in Substoichiometric Titanium Carbide—Correlation with Carbon Vacancy Ordering, *J. Nucl. Mater.*, Vol 169, 1989, p 291-298
17. E. Breval, Microplasticity at Room Temperature of Single Crystal Titanium Carbide with Different Stoichiometry, *J. Mater. Sci.*, Vol 16, 1981, p 2781-2788